plants

MDPI

Review

Driving Electron Transfer in Photosystem I Using Far-Red Light: Overall Perspectives

Jimit Patel [1,†], Amen ElMasadef [2,†], Abraham Peele Karlapudi [3,†], Katayoun Etemadi [2], K. V. Lakshmi [4], Art van der Est [2] and Divya Kaur [1,2,*]

[1] Department of Chemistry, Brock University, St. Catharines, ON L2S 3A1, Canada; jp19fk@brocku.ca
[2] Department of Biological Sciences and Biotechnology, Brock University, St. Catharines, ON L2S 3A1, Canada; ae19ry@brocku.ca (A.E.); ke22ou@brocku.ca (K.E.); avanderest@brocku.ca (A.v.d.E.)
[3] Department of Biotechnology, Vignan's Foundation for Science, Technology and Research, Guntur 522213, Andhra Pradesh, India; abrahampeelekarlapudi@gmail.com
[4] Department of Chemistry and Chemical Biology, The Baruch '60 Center for Biochemical Solar Energy Research, Rensselaer Polytechnic Institute, Troy, NY 12180, USA; k.lakshmi04@gmail.com
* Correspondence: dmatta@brocku.ca
† These authors contributed equally to this work.

Abstract

Photosystem I (PSI) is a photosynthetic protein–pigment complex that, upon photoexcitation, transfers electrons to ferredoxin, facilitating the production of NADPH. Isolated PSI reaction centers (RCs) have also been used in hybrid systems to reduce protons and produce 'biohydrogen'. This review article examines how various cyanobacteria with similar photosynthetic machinery utilize different wavelengths of light to execute photosynthetic electron transport through PSI. Key factors, such as, the structure of the electron transfer cofactors, the protein environment surrounding the primary donor pigments and hydrogen-bonding interactions with the surrounding protein matrix are analyzed to understand their roles in maintaining efficient electron transfer when it is driven using photons of different energies. We compare PSI complexes with known atomic structures from four species of cyanobacteria, *Thermosynechococcus elongatus*, *Acaryochloris marina*, *Halomicronema hongdechloris*, and *Fischerella thermalis*. *T. elongatus* is typical of most oxygenic photosynthetic organisms in that it requires visible light and uses only chlorophyll *a* (Chl *a*) in PSI. In contrast, *H. hongdechloris* and *F. thermalis* are photoacclimating species capable of producing Chl *f* and Chl *d* that use red light when little visible light is available. *A. marina*, on the other hand, is adapted to red light conditions and consistently utilizes Chl *d* as its primary photosynthetic pigment, maintaining a stable pigment composition. Here, we explore the structural and functional differences between the PSI RCs of these organisms and the impact of these differences on electron transport. The structural differences in the cofactors influence both the absorption wavelengths of the cofactors and the energy levels of the intermediate states of electron transfer. An analysis of the surrounding protein shows how it has been adapted and underscores the interplay between the pigment structure, protein environment, and hydrogen bonding networks in tuning the efficiency and adaptability of photosynthetic mechanisms across different species of cyanobacteria.

Keywords: far-red photosynthesis; Photosystem I; reaction center; electron transfer reaction; far-red light photoacclimation; FaRLiP

check for updates

Academic Editor: Katya Georgieva

Received: 24 September 2025
Revised: 27 October 2025
Accepted: 29 October 2025
Published: 5 November 2025

Citation: Patel, J.; ElMasadef, A.; Karlapudi, A.P.; Etemadi, K.; Lakshmi, K.V.; van der Est, A.; Kaur, D. Driving Electron Transfer in Photosystem I Using Far-Red Light: Overall Perspectives. *Plants* **2025**, *14*, 3384. https://doi.org/10.3390/plants14213384

Copyright: © 2025 by the authors. Licensee MDPI, Basel, Switzerland. This article is an open access article distributed under the terms and conditions of the Creative Commons Attribution (CC BY) license (https://creativecommons.org/licenses/by/4.0/).

1. Introduction

Efficient utilization of incident light is crucial for the survival of photosynthetic organisms, which have evolved various strategies to adapt to changes in the wavelength and intensity of light. In this review, we discuss the far-red light acclimation and adaptation strategies that have resulted in different forms of PSI from distinct species of cyanobacteria. However, prior to delving into the details, we present an overview of the light reactions and electron transport cofactors, highlighting recent advances in the field.

1.1. Oxygenic Photosynthesis

Oxygenic photosynthesis is the principal mechanism by which sunlight is converted into chemical energy, making it one of the most fundamental biological processes [1–3]. Cyanobacteria or their early ancestors were the first organisms to perform oxygenic photosynthesis, using water as an electron donor and releasing dioxygen. While dioxygen is key to sustaining aerobic life on the Earth, its production by early oxygenic photosynthetic organisms led to what is known as the Great Oxygenation Event that nearly caused the extinction of all life [1,4,5].

In oxygenic photosynthesis, two distinct photosystems, Photosystem II (PSII) and Photosystem I (PSI) [6], perform light-induced electron transfer to convert light energy into chemical energy. The oxidizing and reducing species generated by electron transfer are used to produce NADPH and dioxygen. The proton transfer that accompanies the electron transfer is used to drive the synthesis of ATP [6–9]. The reducing equivalents stored as NADPH and ATP are subsequently used for CO_2 fixation in the dark reactions [2]. The evolution of photosynthesis has been a complex process that has unfolded over billions of years from primitive anoxygenic bacteria to oxygenic cyanobacteria, algae, and, ultimately, higher plants [10–13]. In eukaryotic organisms, the photosynthetic apparatus is housed in chloroplast organelles resulting from an endosymbiotic relationship between a cyanobacterium and a non-photosynthetic microorganism [14].

1.2. Far-Red Light Photosynthesis

One of the main challenges facing photosynthetic organisms is responding to the changes in the light conditions. The wavelengths and intensity of the incident light vary in different environments and is subject to rapidly change. Different adaptation strategies allow these organisms to deal with these challenges. For example, green sulfur bacteria employ chlorosomes with exceptionally high absorption cross-sections as antenna that allow the organism to survive in extremely low-light environments [11]. Purple bacteria employ bacteriochlorophylls that absorb photons in the IR region beyond 800 nm, allowing them to live in the deep anaerobic layers of lakes or microbial mats with little visible light [15]. Oxygenic photosynthetic organisms have evolved mechanisms that primarily deal with changing light intensity. Cyanobacteria, for example, can undergo state transitions in which the flow of excitation energy from the phycobilisome antenna to the photosystems is altered under different light conditions [16]. These organisms can also alter the ratio of Chl *a*, which absorbs mostly violet and orange light, to Chl *b*, which absorbs mostly blue and yellow light, to adapt their absorption profiles. For many years, it was thought that oxygenic photosynthesis required the absorption of photons in the visible region to provide sufficient energy to drive water oxidation. However, the discovery of the cyanobacteria *A. marina* and *H. Hongdechloris* containing Chl *d* and Chl *f*, respectively, demonstrated that cyanobacteria can also thrive under far-red light conditions [17,18].

Recent advances have provided insight into the molecular diversity and evolutionary pathways of far-red light photosynthetic organisms [19]. Advanced crystallographic

and biochemical analyses reveal the details of the mechanisms underlying the red shift of the photosynthetic pigments. For example, a recent study demonstrated that in allophycocyanins, the light-harvesting proteins found in cyanobacteria, are red-shifted as a result of altered protein–cofactor interactions that lead to a conformational change in the phycocyanobilin chromophore [20,21]. Such knowledge has the potential to allow for the engineering of photosynthetic organisms that utilize a broader spectrum of light, thus improving both efficiency and adaptability and paving the way for innovations in agriculture and biotechnology [20,22].

The term far-red photosynthesis is used to refer to the use of light in the far-red infrared region (700–800 nm) [23] in oxygenic organisms [23,24]. Cyanobacteria, which normally only use the visible part of the spectrum, can perform far-red photosynthesis through two related mechanisms involving Chl molecules that differ in their substituent groups [25]. The first is the adaptation of certain strains of cyanobacteria to niche environments where the incident light is consistently in the far-red region. In this case, the organisms synthesize long wavelength absorbing chlorophyll molecules, such as, Chl *d*, and PSI and PSII adapt to specifically bind these cofactors. The second is a dynamic process in which the organism responds to changes in the light conditions, upregulating the synthesis of modified chlorophylls, such as, Chl *d* and Chl *f* and modified versions of the photosynthetic proteins to bind the pigments when needed through a process known as far-red light photoacclimation (FaRLiP) [23,26–28] (Figure 1).

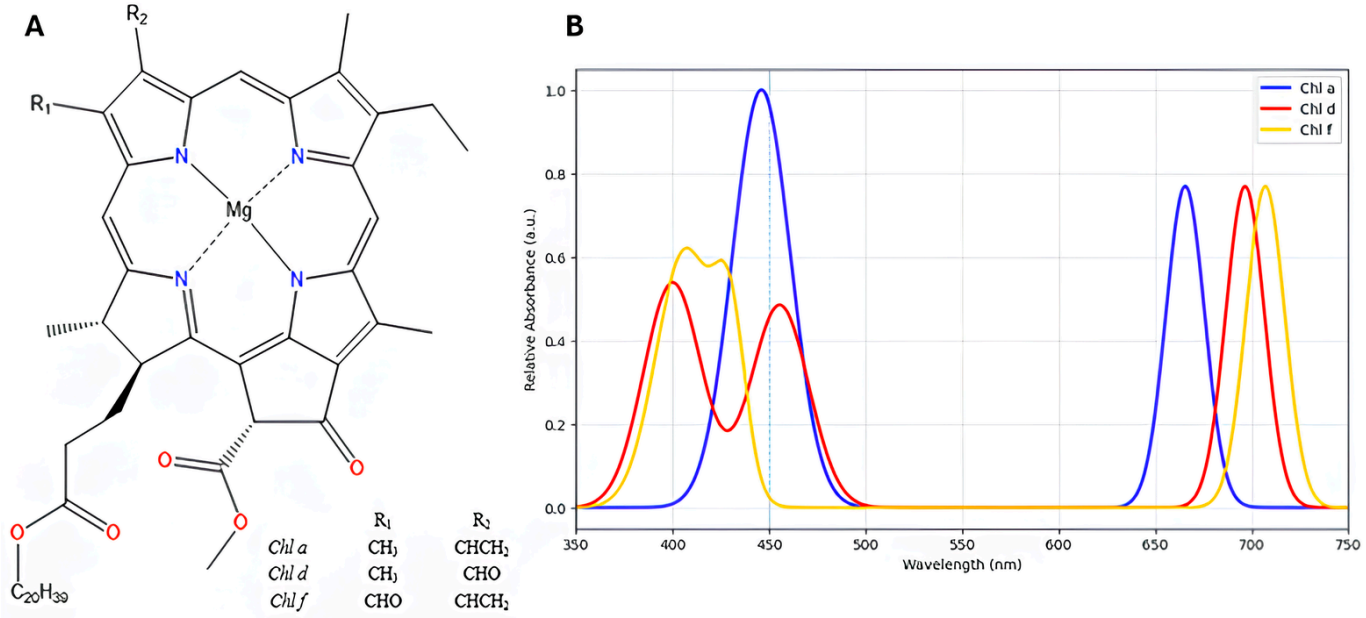


Figure 1. (**A**) Chemical structures of chlorophyll *a*, *d*, and *f*. (**B**) Absorbance spectra generated using the experimental extinction coefficient values of chlorophyll *a*, *d* and *f* in 100 % methanol, as reported in Table 2 of Li et al. (2012) [29]. The experimental spectrum and λ_{max} values can be found in Figure 1 and Table 2, respectively, of the reference Li et al. (2012) [29].

The acclimation and adaptation of photosynthetic organisms to FRL has been reviewed extensively in the literature [17,30–33]. These reviews are focused on the sensing and response to FRL and the evolution of these mechanisms. However, the use of FRL photons has consequences for the energetics of electron transfer in the RCs. With the availability of the near-atomic resolution structures of the RCs, it is now possible to investigate the adaptation of the electron transfer cofactors and the respective binding sites in greater detail. Here, we review the structure of PSI isolated from red-shifted cyanobacterial species and the impact of far-red absorbing Chl molecules on the electron transport chain. We

begin with a brief overview of the structure of the electron transport chain of PSI from the Chl *a*-containing cyanobacterium *T. elongatus*.

1.3. Structure and Electron Energy Transfer in Far-Red-Light-Adapted Photosystem I

PSI from *T. elongatus* contains 12 protein subunits that bind to 96 Chl *a* molecules, 22 carotenoids, 3 four-iron–four-sulfur [4Fe4S] clusters, and two phylloquinone molecules [5]. The core of the RC is a protein heterodimer comprising the membrane-spanning polypeptides PsaA and PsaB that house most of the electron transport cofactors (Figure 2). The pair of chlorophyll molecules labeled eC-A1 and eC-B1 that are shown in blue near the lumenal side of the RC act as the primary electron donor P_{700}. eC-B1 is Chl *a* molecule, while eC-A1 is Chl *a*′, the $C13^2$-epimer of Chl *a*. Two nearly symmetrical branches of cofactors extend across the membrane from P_{700}, each containing two Chl *a* molecules (shown in green and blue in Figure 2) and a phylloquinone molecule (shown orange). The A- and B-branch of cofactors converge at the [4Fe4S] cluster F_X and the terminal [4Fe4S] clusters F_A and F_B are bound to the PsaC subunit on the stromal side of the complex.

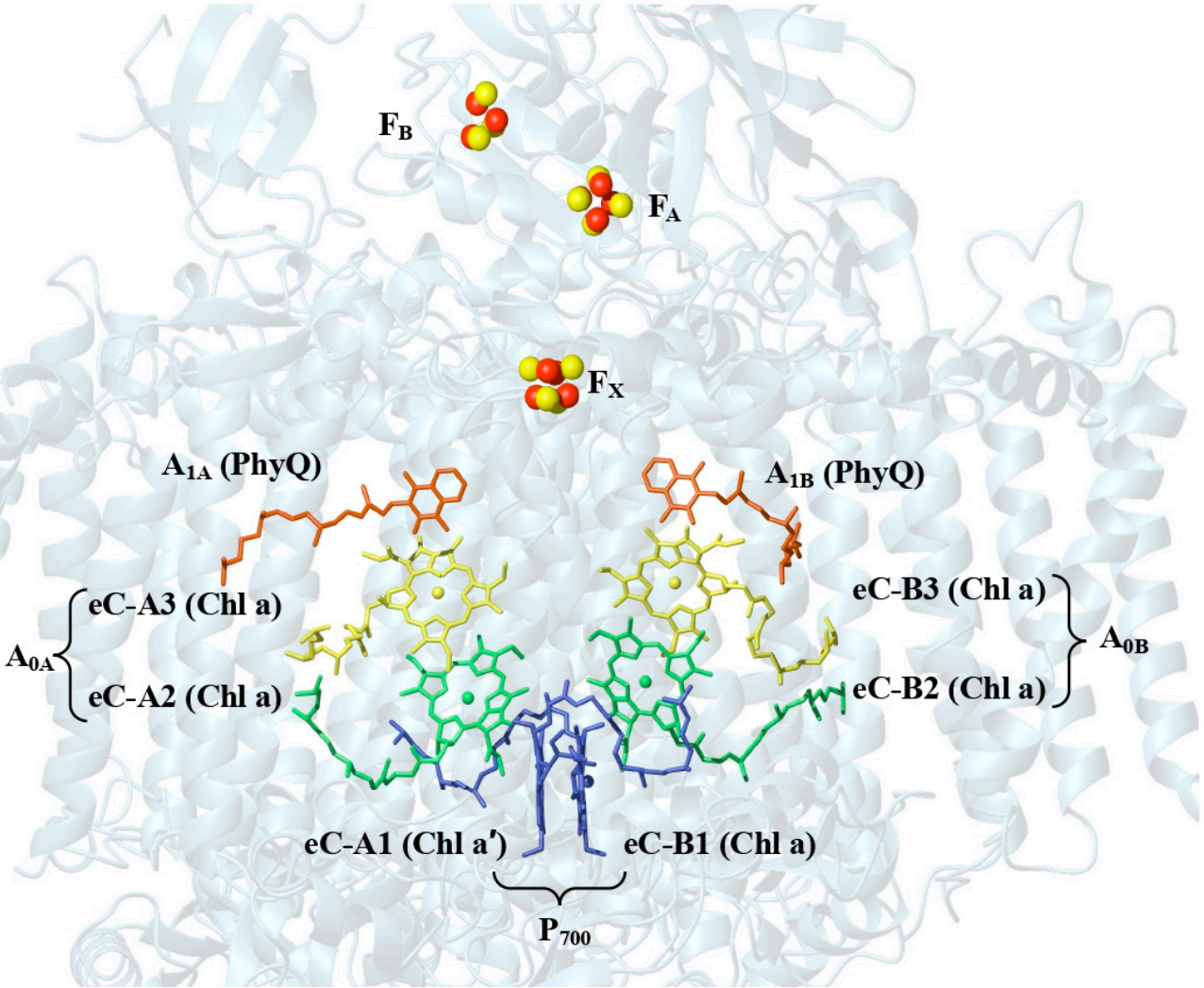


Figure 2. Arrangement of the cofactors that participate in the electron transfer chain of *T. elongatus* (PDB. ID: 1JB0) [9].

Photoexcitation of the primary donor results in electron transfer from P_{700} to F_X in both the A- and B-branch [34]. A variety of models have been proposed for the initial steps of this process [35,36]. However, there is general agreement that the charge-separated state $P_{700}{}^{+}A_{0A}{}^{-}$ or $P_{700}{}^{+}A_{0B}{}^{-}$ is formed within a few picoseconds in either the A- or B-branch. In photo-accumulation experiments, it has been shown that the transferred electron is distributed over two Chl *a* molecules. Thus, we refer to the pair of Chl *a* molecules eC-2 and eC-3 in each branch as the primary acceptor A_0 [7]. Subsequent electron transfer to the phylloquinone acceptors A_{1A} and A_{1B} [37] and the three [4Fe-4S] clusters F_X, F_A, and F_B stabilizes the initial charge separation providing sufficient time for the diffusion limited reduction of $P_{700}{}^{+}$ by soluble plastocyanin and the transfer of the electron from the reduced $(F_A/F_B)^{-}$ clusters to soluble ferredoxin or flavodoxin [38,39]. The distance between the cofactors and their redox potentials are finely tuned to optimize the electron transfer resulting in a quantum yield of near unity. The efficient production of the reductant NADPH is used to drive CO_2 fixation [38]. It is known from a large body of site-directed mutagenesis and quinone exchange studies that even small changes in the cofactors or the protein environment typically lead to impairment of function [40,41]. Thus, it is of interest to understand how PSI RCs from organisms using FRL maintain highly efficient electron transfer processes.

2. Chl *d* Containing PSI

In the marine cyanobacterium *A. marina*, red light-absorbing Chl *d* accounts for 91–97% of the chlorophyll [39,42]. The remaining 3–9% is Chl *a* [43]. *A. marina* was discovered in 1996 when it was extracted from *Lissoclinum patella*, a colonial ascidian collected from the coast of Palau islands in 1993 [16]. Since then, many other strains of *Acaryochloris* have been discovered to use far-red light to drive the photosynthetic reactions [44]. These strains differ in the specific wavelengths of far-red light used, which has enabled adaptation to diverse ecological environments [45]. While most of them are known to utilize far-red light, *A. marina* MBIC11017 has been shown to acclimate to white light by altering the ratio of PSI:PSII and increasing the number of phycobilisomes [46]. In PSI from *A. marina*, the absorption maximum of the primary donor P_{740} is red-shifted to 740 nm as a result of the presence of Chl *d* [46]. This change raises intriguing questions about its effect on the energetics of electron transport and the structure–function relationships. The recent cryo-EM structure of PSI from *A. marina* with a resolution of 2.58 Å published by Hamaguchi et al. [41]. facilitates detailed comparisons of the electron transfer cofactors of *T. elongatus* and *A. marina*.

2.1. Electron Transport Chain (ETC) of Acaryochloris marina PSI

In *T. elongatus*, P_{700} is a Chl *a*/Chl *a*′ heterodimer and A_0 is a Chl *a* homodimer. In contrast, P_{740} is a Chl *d*/Chl *d*′ heterodimer [47,48], and the eC-2 and eC-3 cofactors in each branch are a Chl *d* and pheophytin, respectively, in *A. marina*. The phylloquinones, A_{1A} and A_{1B}, and three [4Fe4S] clusters F_X, F_A, and F_B are similar in both organisms. Despite the differences in some of the cofactors, the arrangement of these pigments is identical in *A. marina* and *T. elongatus* [39].

2.2. Absorption Characteristics of P_{740}

The change in the vinyl group substituent at the C3 position of Chl *a* to a formyl group in Chl *d* (Figure 1) causes a red shift of 25 nm in the Qy absorption band measured in acetone [49]. Qualitatively, this effect can be attributed to the stabilization of the lowest unoccupied molecular orbital (LUMO) due to greater delocalization onto the more electronegative formyl group [50]. In the protein environment, the Qy absorption maxima of P_{700} and P_{740} are both red-shifted compared to the respective Chls in organic solvents as a result of the excitonic interactions between the chlorophylls of the respective dimers and protein cofactor interactions. The Qy maximum for P_{700} is shifted by ~800 cm^{-1} compared to Chl *a* in solution, whereas the shift for P_{740} relative to Chl *d* in vitro is ~1000 cm^{-1}. Thus, although the different substituent groups of the Chl are responsible for the red shift of P_{740}, a difference in the interaction between the two Chls in the dimer and/or a difference in the influence in the protein environment also appears to play a role. The metal coordination properties of the central Mg^{2+} ion of Chl *a* and Chl *d* are similar [51], and the nature and arrangement of the axial His ligand of P_{740} and P_{700} are essentially the same in the respective X-ray crystal structures. This suggest that the change in vinyl to formyl at the C3 position does not affect the binding to protein [25,47]. Nonetheless, protein-cofactor interactions are expected play an important role in tuning the electronic properties of P_{740}.

2.3. The Midpoint Potential and Electronic Asymmetry of P_{740}

The midpoint potential (E_m) of the primary donor P_{740} has been estimated as +425–+450 mV [48,52,53] vs. SHE. This is well within the +400–+470 mV range for the E_m of P_{700} in Chl *a*-containing cyanobacteria [54]. In contrast, the midpoint potential of Chl *a* and Chl *d* in vitro in acetonitrile are +810 mV and +880 mV, respectively, [55]. The lower E_m values of P_{740} and P_{700} in vivo can be ascribed to greater stabilization of the oxidized dimer in the protein environment compared to the corresponding oxidized monomers in solution. The protein sequence and structure in the vicinity of P_{740} and P_{700} are highly conserved in *A. marina* and *T. elongates*, suggesting similar stabilization in vivo. Within the uncertainty of the reported midpoint potentials, it appears that the higher oxidation potential of Chl *d* compared to Chl *a* (~70 mV) observed in solution is compensated for by subtle differences in the chlorophyll and/or chlorophyll–protein interactions in P_{700} and P_{740}. It is not surprising that these interactions result in similar E_m of P_{740}^{+} and P_{700}^{+}, since both are re-reduced by the same soluble electron donors, plastocyanin or cytochrome *f*.

The structure of P_{740} in PSI from the *A. marina* and the surrounding protein environment is shown in Figure 3A. Here, eC-A1 is a Chl *d*′ molecule and the eC-B1 is Chl *d* and there are three water molecules in the vicinity of eC-B1. The water molecules form putative hydrogen bonds with the neighboring amino acid residues Tyr601A, Ser605A, Asn608A, Ser741A, Tyr745A, and Chl *d*′ [39]. In contrast, PSI from *T. elongatus* contains just one water molecule in the vicinity of P_{700}, that possibly forms hydrogen bonds with Tyr603A, Ser607A, Thr743A, and Chl *a*′ (Figure 3B) [6].

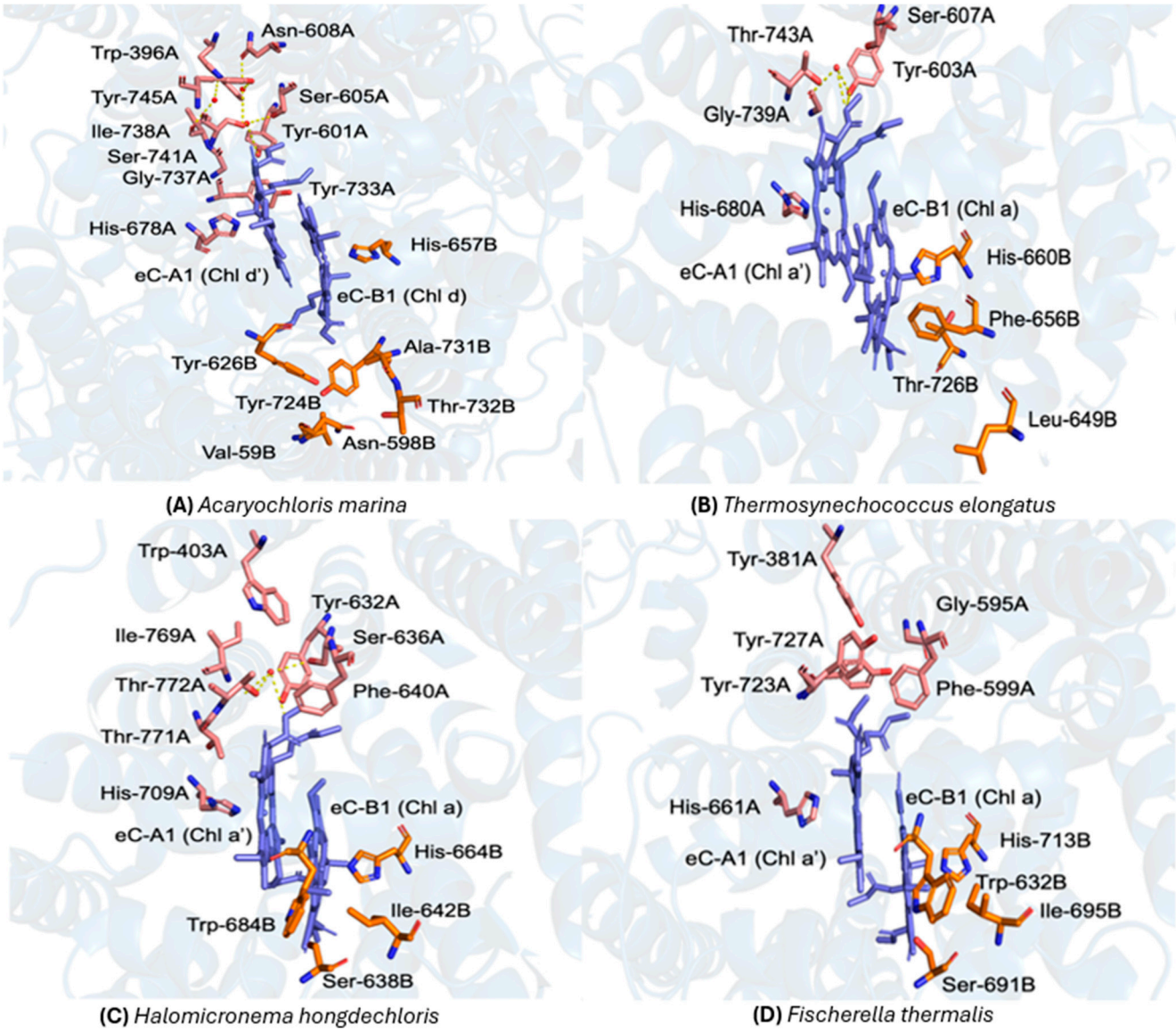


Figure 3. Comparison of the primary donor sites and their local protein environments in Photosystem I (PSI) from four cyanobacterial species. (**A**) *Acaryochloris marina* (P740; PDB ID: 7COY) [39]: the Chl *d*′ (eC-A1) and Chl *d* (eC-B1) molecules are shown in blue, with surrounding residues from P_A and P_B depicted in pink and orange, respectively, and this color scheme is applied to all organisms in this study. Key A-branch residues include Trp-396A, Ile-738A, Asn-608A, Tyr-601A, Ser-605A, Tyr-733A, Tyr-745A, Ser-741A, and Gly-737A, coordinated by His-678A; B-branch residues include Tyr-724B, Ala-731B, Thr-732B, Val-594B, Asn-598B, and Tyr-626B, coordinated by His-657B. Three nearby water molecules (red spheres) and their putative hydrogen bonds (yellow dashed lines) are indicated [39]. (**B**) *Thermosynechococcus elongatus* (P700; PDB ID: 1JB0) [6]: Chl *a*′ (eC-A1) and Chl *a* (eC-B1) are shown in blue. The A-branch includes Tyr-603A, Ser-607A, Gly-739A, Thr-743A, and His-680A, while the B-branch comprises Phe-656B, Leu-649B, Thr-726B, and His-660B. A water molecule (red sphere) and its hydrogen-bond network (yellow dashed lines) illustrate stabilizing interactions near the donor [6]. (**C**) *Halomicronema hongdechloris* (P700; PDB ID: 6KMX) [56]: Chl *a*′ (eC-A1) and Chl *a* (eC-B1) are shown in blue. The water molecule is shown as a red sphere. (**D**) *Fischerella thermalis* (PDB ID: 7LX0): the primary donor environment closely resembles that of *H. hongdechloris* [57]. At the reported 2.96 Å resolution, only strongly bound waters could be modeled; thus, the apparent absence of water or hydrogen-bond interactions likely reflects limited structural resolution rather than a true lack of water molecules [58].

The differences in the hydrogen (H) bonding network in the vicinity of P_{700} and P_{740} may be responsible for maintaining the midpoint potential and is expected to influence the asymmetry of the charge distribution. In *C. reinhardtii*, site-directed mutagenesis studies have shown that altering the axial His ligand to eC-B1 changes the midpoint potential of P_{700} and the unpaired electron spin density distribution of the P_{700}^{+} radical cation [59]. Corresponding changes to the axial His ligand of eC-A1 had no effect. Thus, it was concluded that the charge and unpaired electron spin density distribution on P_{700}^{+} is primarily localized on the eC-B1 chlorophyll. Since H-bonds have an electron withdrawing effect, it is expected that the asymmetric H-bonding to P_{700}^{+} would draw electron density towards the Chl with more and/or stronger H-bonding interactions, leading to the localization of positive charge density on the other Chl [60,61]. Indeed, it has been shown in purple bacterial reaction centers that there is a linear correlation between the midpoint potential and the total enthalpy of the hydrogen (H)-bonds to the carbonyl groups of the primary donor chlorophylls [60]. Thus, the larger number of water molecules and H-bonding interactions in the vicinity of eC-A1 in *A. marina* might be expected to result in a higher midpoint potential and higher electron hole localization on eC-B1 in P_{740}^{+} compared to P_{700}^{+}. Based on a computational study combining electrostatic continuum calculations and QM/MM methods by Saito et al. (2011) [62], the *Em* of Chl *a* and Chl *a*′ of P_{700} suggested an eC-A1$^{\bullet+}$: eC-B1$^{\bullet+}$ ratio of 28:72 due to the strong putative H-bond between P_A and Thr743A as one of the main factors. A study of the molecular geometry and vibrational frequency using DFT methods employing a B3LYP functional and a6-31G(d) basis set with a PCM solvent model calculated the eC-A1$^{\bullet+}$:eC-B1$^{\bullet+}$ ratio of P_{740} as 60:40, without specifying the branching ratio [63]. However, computational and electron nuclear double resonance (ENDOR) studies show that the electron spin density distribution of P_{740}^{+}+ and P_{700}^{+} are similar, which suggests that the difference in the number of water molecules and the H-bonding interactions have a relatively minor effect [64]. More research is needed to better understand the underlying reasons for the asymmetric electron transfer and asymmetry of spin and charge distribution in the two organisms.

2.4. Electron Transfer Energetics and the Protein Environment

The local protein environment surrounding the Chls that form the dimeric primary acceptor A_0 and the secondary phylloquinone acceptor A_1 is also conserved in PSI from the different species of cyanobacteria, except for the axial ligands of eC-3. In PSI from *T. elongates*, eC-3A and eC-3B are ligated by Met688A and Met668B, respectively. However, eC-3A and eC-3B are pheophytin molecules in *A. marina* PSI lacking a central Mg(II) ion and therefore do not contain axial ligands [65]. The Met residue in the A-branch coordinated to eC-3A in *T. elongatus* is conserved *A. marina* PSI; however, the corresponding residue in the B-branch of *A. marina* is a Leu. This difference does not appear to significantly impact the rate of electron transfer in the two branches in *A. marina*. This is in stark contrast to PSI from *T. elongatus* and *C. reinhardtii*, where mutation of Met688A and Met668B profoundly affects the electron transfer rates [66–68]. A recent study of the initial charge separation kinetics by Petrova et al. [65] suggests that the use of Pheo as the A_0 acceptor in *A. marina* is necessary to provide the driving force required for forward electron transfer from P_{740}. The difference in the absorption wavelength suggests that the excited state P_{740}* is ~100 meV lower in energy than P_{700}* relative to the respective ground states. Therefore, this loss in excitation energy must be compensated for by lowering the energy of the charge-separated state. Since the midpoint potential of P_{700} and P_{740} are similar, the energy of the charge-separated state can only be lowered by rendering the midpoint potential of the primary acceptor more positive. Ultrafast optical spectroscopy has suggested that the midpoint potential of Pheo in

A. marina is ~100 mV more positive than A_0 in *T. elongatus*. However, the uncertainty in this estimation is fairly large because the values obtained depend on the assumed mechanism of the initial charge separation and stabilization used in the analysis. A recent study by Noji et al. [69] addressed this issue by solving the linear Poisson–Boltzmann equation to estimate the midpoint potential for the electron transfer cofactors. They found that the midpoint potential of eC-2A is ~200 mV more positive in *A. marina* than in *T. elongatus*. However, if the calculation is repeated using the *A. marina* structure with Chl *a* in the binding site, the midpoint potential is essentially the same as that in *T. elongatus*. Hence, it appeared that the difference in the midpoint potential is inherent to the chemical structure of the Chl and does not arise from differences in the protein environment. Similarly, the midpoint potential of eC-3 (Pheo-A) in *A. marina* is ~200 mV more positive than eC-3 (Chl *a*) in *T. elongatus*. Thus, the change from Chl *a* in *T. elongatus* to Pheo-A in *A. marina* keeps eC-3$^-$ energetically lower than the eC-2$^-$.

The secondary phylloquinone acceptors, A_{1A} and $A_{1B,}$ are similar in *A. marina* and *T. elongatus*. In both organisms, the quinones are involved in hydrophobic interactions with a tryptophan and Leu residue and form a single putative hydrogen bond to a backbone NH group. In *T. elongatus*, the H-bonding partners are Leu722A and Leu706B, respectively, [6]. In other cyanobacteria, such as, *Gloeobacter*, the putative hydrogen bond in the B-branch is a Met [70]. This pattern is reversed in *A. marina*, where A_{1A} forms a putative hydrogen bond to Met720A while A_{1B} to Leu665B.

The conformation of the phytyl tail of the phylloquinone in the A_{1B} site differs in *A. marina* and *T. elongatus* [39,42]. Shen and coworkers speculate that this may arise from structural changes as Met acts as the axial ligand to A_0 in *T. elongatus* and Leu in *A. marina* [42]. Not surprisingly, the terminal [4Fe4S] clusters in *A. marina* are nearly identical to those in *T. elongatus*, indicating that the midpoint potentials and electron transfer properties are likely unaffected by the other changes in the electron transfer chain [39].

3. Far-Red Light Photoacclimation (FaRLiP)

The second class of cyanobacteria that use FRL acclimate to longer wavelengths in a process known as FaRLiP, resulting in the incorporation of Chl *f* [22]. This type of Chl was first identified in the methanol extracts of stromatolites from Shark Bay, Western Australia and its presence led to the discovery of the cyanobacterium *H. hongdechloris*, a FaRLiP species that can sense light conditions and synthesize Chl *f* when needed [18,43,71–73]. The ability of these organisms to adapt to FRL was first discovered by Bryant and coworkers in the filamentous, non-heterocystous cyanobacterium *Leptolyngbya* sp. JSC-1 isolated from microbial mats in hot spring pools [74]. They found that this species acclimates dynamically to far-red light by remodeling PSI, PSII and phycobilisome proteins and their cofactors [27,30,31,75,76]. These alterations are associated with a cluster of genes that has now been identified in up to twenty species of cyanobacteria [31,32]. This gene cluster is highly conserved and consists of approximately twenty genes that encode for paralogs of the subunits of PSI, PSII, and phycobillisomes as well as the enzymes required for Chl *f* and Chl *d* biosynthesis [32,76]. The absorption of FRL by the phytochrome RfpA is thought to initiate a series of steps that lead to the activation of the regulator/transcription activator RfpB. The activated form of RfpB then activates the transcription of these genes to produce components of the photosynthetic apparatus optimized for FRL [77].

3.1. Characterization of Chl f-Containing Photosystems

The Chl *f* content in *H. hongdechloris* and *F. thermalis* varies depending on the wavelengths of the light under which the cultures are grown. Under white light, Chl *f* is minimal, but under FRL, it reaches 8–12.5% of the total amount of Chls [26]. In addition to activating the biosynthesis of Chl *f*, other photosynthetic pigments and proteins, such as the PSI subunits, are also altered [73]. In the modified form of PSI from *F. thermalis* grown under FRL, 6 out of 12 subunits (PsaA1, PsaB1, PsaL1, PsaI1, PsaF1, and PsaJ1) are replaced by alternative versions (PsaA2, PsaB2, PsaL2, PsaI2, PsaF2, and PsaJ2) that are encoded within the FaRLiP gene cluster [18,19,73,78]. The cryo-em 2.96 Å and cryo-em 3.19 Å structure of PSI from *F. thermalis* and cryo-em 2.41 Å *H. hongdechloris* grown under FRL conditions has shown that the locations of the Chls remain unchanged under FRL. However, several Chl binding sites observed in PSI from *T. elongatus*, and *A. marina* are absent in PSI from FRL *F. thermalis*, which results in the incorporation of Chl *f* as the major pigment. Based on the total Chl *f* content, ~7–8 Chl *f* molecules are expected to be found in PSI from FRL-acclimated *H. hongdechloris* and *F. thermalis* [28]. An important question is whether the Chl *f* in the FRL-acclimated species are involved in electron transfer. Nürnberg et al. (2018) initially reported biophysical studies of RCs from a FRL adapted cyanobacterium [19,75]. Based on the action spectra, it was proposed that charge separation in both PSI and PSII in *Chroococcidiopsis thermalis* PCC 7203 involves Chl *f*. Since the P_{700} absorbance was not red-shifted and the high midpoint potential of Chl *f* makes it a poor choice for A_0, it was suggested that the accessory Chl site was the location for Chl *f*. Hastings and coworkers (2019) studied PSI from FRL-acclimated *F. thermalis* using FTIR difference spectroscopy, suggesting that P_{700} is a Chl *a*/Chl *a*′ dimer, and provided evidence of Chl *f* in the eC-2 sites [43,72,79]. However, time-resolved optical data spectroscopy indicates that the time scale on which the secondary charge separated states are formed following Chl *f* excitation is inconsistent with their participation in the electron transfer chain [80].

Determining the locations of Chl *f* in PSI from *H. hongdechloris* and *F. thermalis* is challenging as the resolution of the cryo-EM density maps is not sufficient to unequivocally distinguish between the formyl group of Chl *f* and the corresponding methyl group of Chl *a* [28]. Moreover, it is possible that a fraction of the sites in PSI from *F. thermalis* contain Chl *f* while the remainder are occupied by Chl *a*. Nonetheless, in PSI from *H. hongdechloris* and *F. thermalis* seven of the 96 and 89 Chls, respectively, were modeled as Chl *f*, all of which were located in the antenna [22,26,81]. In *H. hongdechloris*, six of the seven Chl *f* molecules were assigned to a network on the PsaA2 side of the complex near the interface with one of the two neighboring PSI complexes in the trimer. In *F. thermalis*, the lower resolution made the assignment more challenging and four possible binding sites were tentatively identified in the antenna. Most of the changes in the protein structure were due to alterations in amino acid side chains that allowed space for or provided putative hydrogen bond donors to the formyl oxygen on the A ring of Chl *f*. Additionally, several loop insertions and deletions were found in both structures. The assignment of Chl *f* only to antenna binding sites contradicted the earlier spectroscopic evidence suggesting that one or both of the accessory Chls of the electron transfer chain may be Chl *f* [79,82,83]. However, a rigorous analysis of the electron density maps taking into account the local energy landscape, the presence of possible hydrogen bond donors, and the nature of the axial ligand to the Chls has provided evidence for the locations of Chl *f* in the antenna [84].

3.2. The Electron Transfer Chain in FRL-PSI from H. hongdechloris and F. thermalis

The electron transfer cofactors in *H. hongdechloris* and *F. thermalis* are similar to those of *T. elongatus*, including the pseudo-C_2 symmetric arrangement of the cofactors in the A- and B-branch, meaning that the electron transfer cofactors in the A- and B-branches are arranged with near-two-fold rotational symmetry around an axis normal to the membrane plane. This rotational symmetry is not exact because the protein environments in the two branches differ and there are slight differences in the orientations of the cofactors. The primary donor Chls eC-A1 and eC-B1 are directly ligated by His709A and His664B, respectively, in *H. hongdechloris* PSI (Figure 3C).

As is the case in PSI from *T. elongatus*, only one water molecule is present in the vicinity of P_A in PSI from FRL-acclimated *H. hongdechloris*, which forms putative hydrogen bonds with the Ser636A, Tyr632A, Gly768A, Thr772A, and methoxy O-13 group of P_A [26]. The P_B Chl of *H. hongdechloris* does not participate in hydrogen bonding [85]. The amino acids participating in hydrogen bonding around Chl *a*′ are also conserved in PSI from *H. hongdechloris* and *T. elongatus*. Thus, the energetics of electron transfer appears to be unaltered in FRL-acclimated PSI.

Another factor that can influence the energetics is the orientation of the pigments [7,86,87]. The fact that the orientation of eC-A1 and eC-B1 in P_{700} from *H. hongdechloris* and *T. elongatus* are virtually identical suggests that there is no significant difference in the E_m and energetics of electron transfer. The excited state from which electron transfer is initiated is higher in energy than the available photons under FRL conditions, which suggests that electron transfer must be coupled to uphill energy transfer from Chl *f* on the periphery of the complex to P_{700} in the core [25].

3.3. Excitation Energy Transfer

The apparent lack of any change in the energetics in the electron transfer in PSI from FRL-acclimated *H. hongdechloris* and *T. thermalis* raises the intriguing question of how photons with less energy than that required for the photoexcitation P_{700} can initiate electron transfer. The input required for energy transfer from Chl *f* at 810 nm to Chl *a*, is ~770 cm^{-1} and well above thermal energy at ambient temperature. This implies that the energy transfer is coupled to low-frequency vibrational modes and since the Boltzmann factor describing the probability of excitation of such modes is 0.025, the uphill energy transfer is expected to be slow. Indeed, there is evidence that the energy transfer in photosystems containing red-shifted Chls is a two-step process in which the excitation is initially trapped on the red-shifted Chl, followed by slower uphill energy transfer [88]. Nonetheless, the rates of energy transfer are faster than expected and mathematical modeling suggests that the uphill energy transfer is entropy-driven. Because the ratio of Chl *f*/Chl *a* in the antenna is small, there are a large number of possible pathways for energy transfer from Chl *f* to Chl *a* [22]. Since the number of pathways is related to the probability of energy transfer, a small Chl *f*: Chl *a* ratio has been proposed to partially compensate for the intrinsically low probability of uphill transfer [89].

3.4. Comparative Analysis of the Protein Environment Surrounding P_{700} in H. hongdechloris, F. thermalis and T. elongatus

A recent comparative analysis of the protein environment of PSI from *F. thermalis* and *H. hongdechloris* revealed a high degree of structural similarity. However, a key distinction is in the absence of water molecules in PSI from *F. thermalis*, as observed in the cryo-EM 2.96 Å and 3.19 Å structure (PDB ID: 6PNJ, [90] 7LX0) [57]. While this observation pertains to the PSI core, it is important to note that Chl *f* molecules are localized at the periphery of the antenna, spatially distant from the electron transfer chain [22,28].

This raises the question of whether differences in the hydration state in the PsaA and PsaB subunits plays a functional role in FRL acclimation. Structural comparisons between *F. thermalis* and *H. hongdechloris* indicate only minor variations in the orientations of the amino acid side chains near the core, typically within 1 Å. Thus, while the absence of water molecules in the core is a noteworthy structural feature, its direct impact on FRL-driven electron transfer remains uncertain, especially given the peripheral location of Chl *f*.

To evaluate sequence conservation within the local protein environments surrounding the primary donor branches, residues located within a 15 Å radius of the central Mg atom of the reaction center chlorophylls in both the A and B-branches were selected. This distance ensures inclusion of all amino acids potentially contributing to electron transfer. Residues within this cutoff were first identified from the *T. elongatus* structure and subsequently used as a reference for cross-species alignment. Conservation was assessed by comparing the total number of residues per branch with the number of identical residues at corresponding positions in *A. marina*, *H. hongdechloris*, and *F. thermalis*. The percentage of conservation was then calculated as the ratio of identical to total residues. Based on this analysis, *A. marina* exhibited 79% conservation in the A-branch and 68% in the B-branch, *H. hongdechloris* showed 79% conservation in both branches, and *F. thermalis* displayed 80% and 77% conservation in the A and B-branches, respectively, (Figure 4). Nevertheless, several amino acids surrounding the primary donor in PSI from *T. elongatus*, *A. marina*, *H. hongdechloris* and *F. thermalis* display significant variations. Notably, in the vicinity of P_B, Tyr727 in *F. thermalis* is replaced by Thr743 in *T. elongatus*. Conversely, in the case of P_A Thr776 in *F. thermalis* is substituted by Tyr727 in *T. elongatus*. Additionally, for P_A Ala658 in *T. elongatus* corresponds with Ser635 in *F. thermalis*, while Val661 in *T. elongatus* corresponds to Leu638 in *F. thermalis*. For P_B, Val694 in *F. thermalis* aligns with Leu637 in *T. elongatus*. These critical differences could highlight the variability of amino acids surrounding the primary donor between these two species. Further investigations and an expanded analysis of the protein environment could reveal insightful similarities and differences between the two organisms.

3.5. Comparison of Water Molecules

A comprehensive comparative analysis of the protein environment of *T. elongatus* and *F. thermalis* revealed notable differences, especially in the number and location of water molecules and putative H bonding interactions. A significant distinction is the lack of water molecules in *F. thermalis*. This absence suggests a possible adaption or structural feature that differentiates *F. thermalis* from *H. hongdechloris* and *T. elongatus*, despite general similarities in the protein environments. Analyses utilizing high-resolution structural data (PDB ID: 6PNJ and 7LX0) [57,81] disclose nuanced yet significant variations in the orientation of critical amino acid side chains in the vicinity of the primary donor, P_{700} and P_{740}. The variations, frequently within 1 Å, influence the capacity of the Chls to interact with water molecules or neighboring amino acids.

It appears that the lack of water molecules in *F. thermalis* impairs the formation of the putative H bonding networks that are observed in *T. elongatus*. The Tyr727 residue in *F. thermalis* correlates to Thr743 in *T. elongatus*, with analogous shifts noted for other residues, such as, Ala658 in *T. elongatus* and Ser635 in *F. thermalis*. Additional computational modeling and experimental validation are required to better understand the effects of the structural changes on the stability and efficiency of electron transfer. This could yield insights on the evolutionary adaptation of cyanobacteria to different wavelengths of light and may reveal novel opportunities for bioengineering applications.



Figure 4. Alignment of PsaA sequences (rings) from of *T. elongatus* (PDB ID: 1JB0) [6,91], *A. marina* (PDB ID: 7COY) [39], *H. hongdechloris* (PDB ID: 6KMX) [56] and *F. thermalis* (PDB ID: 7LX0) [57]. Conserved residues are shown in cyan, and non-conserved residues are especially noted in the P700-cofactor environment. Numbering of residues is based on the *T. elongatus* sequence for consistency across species. For example, Thr743A (*T. elongatus*) is Ser in *H. hongdechloris*/*A. marina*, and Ala658A (*T. elongatus*) is Ser in *F. thermalis*. These differences lie adjacent to water-mediated H-bond networks and are expected to influence the hydrogen bonding and electrostatic stabilization of the P700 chlorophylls. The alignment highlights how specific substitutions in far-red–adapted species may tune the PSI protein–cofactor interface.

4. Conclusions

This review provides an overview of the structural differences in PSI of several species of cyanobacteria—specifically *A. marina*, *H. hongdechloris*, and *F. thermalis*— which have evolved to use different wavelengths of light and in the case of *H. hongdechloris* acclimate to far-red light conditions. Perhaps, somewhat surprisingly, the structural differences between PSI from these three species are rather minor. The most significant is the use of pheophytin as the eC-A3 acceptor in *A. marina*, which appears to have occurred to maintain the necessary driving force for forward electron transfer when the absorption wavelength of the donor is lowered. However, there are also subtle differences in the hydrogen bonding networks and the arrangement of water molecules around the primary donors, which may have arisen to fine tune their redox properties.

Interest in the far-red light adaptation of cyanobacteria is driven in part by the possibility of improving crop yields and land use by increasing photosynthetic efficiency at long wavelengths. The fact that cyanobacteria have been able to adapt to low-intensity, long-wavelength light environments, with relatively minor adjustments to their photosynthetic apparatus, suggests that it may be possible to engineer similar traits in higher plants. This could lead to the development of bioengineered crops and algae that can thrive in a wider range of environmental conditions, potentially increasing agricultural productivity and sustainability and addressing global challenges in food security and sustainable energy production.

Author Contributions: Conceptualization and investigation, D.K.; writing—original draft preparation J.P., A.E., A.P.K., K.E. and D.K.; reviewing and editing, D.K., K.V.L. and A.v.d.E. All authors have read and agreed to the published version of the manuscript.

Funding: This work was supported by a Discovery Grant from the Natural Science and Engineering Research Council of Canada to DK (Discovery Grant No. 2024-04171, startup funds by Brock University), AvdE (Discovery Grant No. 2015-04021) and by the Photosynthetic Systems Program, Office of Basic Energy Sciences of the U.S. Department of Energy under the contracts DE-FG02-07ER15903 (KVL).

Data Availability Statement: The original contributions presented in this study are included in the article. Further inquiries can be directed to the corresponding author.

Conflicts of Interest: The authors declare no conflicts of interest.

References

1. Nelson, N.; Junge, W. Structure and Energy Transfer in Photosystems of Oxygenic Photosynthesis. *Annu. Rev. Biochem.* **2015**, *84*, 659–683. [CrossRef]
2. Kaiser, E.; Correa Galvis, V.; Armbruster, U. Efficient Photosynthesis in Dynamic Light Environments: A Chloroplast's Perspective. *Biochem. J.* **2019**, *476*, 2725–2741. [CrossRef] [PubMed]
3. Gorka, M.; Landry, P.; Gruszecki, E.; Malnati, A.; Kaur, D.; Van Der Est, A.; Golbeck, J.H.; Lakshmi, K.V. Chlorophylls as Primary Electron Acceptors in Reaction Centers. In *Photosynthesis*; Elsevier: Amsterdam, The Netherlands, 2023; pp. 197–237. [CrossRef]
4. Hohmann-Marriott, M.F.; Blankenship, R.E. Evolution of Photosynthesis. *Annu. Rev. Plant Biol.* **2011**, *62*, 515–548. [CrossRef]
5. McEvoy, J.P.; Gascon, J.A.; Batista, V.S.; Brudvig, G.W. The Mechanism of Photosynthetic Water Splitting. *Photochem. Photobiol. Sci.* **2005**, *4*, 940–949. [CrossRef] [PubMed]
6. Jordan, P.; Fromme, P.; Witt, H.T.; Klukas, O.; Saenger, W.; Krauß, N. Three-Dimensional Structure of Cyanobacterial Photosystem I at 2.5 Å Resolution. *Nature* **2001**, *411*, 909–917. [CrossRef]
7. Gorka, M.J.; Baldansuren, A.; Malnati, A.; Gruszecki, E.; Golbeck, J.H.; Lakshmi, K.V. Shedding Light on Primary Donors in Photosynthetic Reaction Centers. *Biophys. J.* **2022**, *121*, 103a–104a. [CrossRef]
8. Brudvig, G.W.; Beck, W.F.; Paula, J.C. Mechanism of Photosynthetic Water Oxidation. *Annu. Rev. Biophys. Biophys. Chem.* **1989**, *18*, 25–46. [CrossRef]
9. Gorka, M.; Charles, P.; Kalendra, V.; Baldansuren, A.; Lakshmi, K.V.; Golbeck, J.H. A Dimeric Chlorophyll Electron Acceptor Differentiates Type I from Type II Photosynthetic Reaction Centers. *iScience* **2021**, *24*, 102719. [CrossRef]
10. Blankenship, R.E. Early Evolution of Photosynthesis. *Plant Physiol.* **2010**, *154*, 434–438. [CrossRef]
11. Blankenship, R.E.; Olson, J.M.; Miller, M. Antenna Complexes from Green Photosynthetic Bacteria. In *Anoxygenic Photosynthetic Bacteria*; Blankenship, R.E., Madigan, M.T., Bauer, C.E., Eds.; Advances in Photosynthesis and Respiration; Kluwer Academic Publishers: Dordrecht, The Netherlands, 2004; Volume 2, pp. 399–435. [CrossRef]
12. Sager, R.; Ramanis, Z. Recombination of Nonchromosomal Genes in Chlamydomonas. *Proc. Natl. Acad. Sci. USA* **1965**, *53*, 1053–1061. [CrossRef]
13. Keeling, P.J. Diversity and Evolutionary History of Plastids and Their Hosts. *Am. J. Bot.* **2004**, *91*, 1481–1493. [CrossRef] [PubMed]
14. López-Juez, E. Steering the Solar Panel: Plastids Influence Development. *New Phytol.* **2009**, *182*, 287–290. [CrossRef] [PubMed]
15. Miyashita, H.; Ikemoto, H.; Kurano, N.; Adachi, K.; Chihara, M.; Miyachi, S. Chlorophyll d as a Major Pigment. *Nature* **1996**, *383*, 402. [CrossRef]
16. Alcorta, J.; Vergara-Barros, P.; Antonaru, L.A.; Alcamán-Arias, M.E.; Nürnberg, D.J.; Díez, B. Fischerella Thermalis: A Model Organism to Study Thermophilic Diazotrophy, Photosynthesis and Multicellularity in Cyanobacteria. *Extremophiles* **2019**, *23*, 635–647. [CrossRef]
17. Gan, F.; Bryant, D.A. Adaptive and Acclimative Responses of Cyanobacteria to Far-Red Light. *Environ. Microbiol.* **2015**, *17*, 3450–3465. [CrossRef]
18. Gan, F.; Shen, G.; Bryant, D. Occurrence of Far-Red Light Photoacclimation (FaRLiP) in Diverse Cyanobacteria. *Life* **2014**, *5*, 4–24. [CrossRef]
19. Gisriel, C.J.; Bryant, D.A.; Brudvig, G.W.; Cardona, T. Molecular Diversity and Evolution of Far-Red Light-Acclimated Photosystem I. *Front. Plant Sci.* **2023**, *14*, 1289199. [CrossRef]
20. Gisriel, C.J.; Elias, E.; Shen, G.; Soulier, N.T.; Brudvig, G.W.; Croce, R.; Bryant, D.A. Structural Comparison of Allophycocyanin Variants Reveals the Molecular Basis for Their Spectral Differences. *Photosynth. Res.* **2024**, *162*, 157–170. [CrossRef]
21. Zhou, L.-J.; Höppner, A.; Wang, Y.-Q.; Hou, J.-Y.; Scheer, H.; Zhao, K.-H. Crystallographic and Biochemical Analyses of a Far-Red Allophycocyanin to Address the Mechanism of the Super-Red-Shift. *Photosynth. Res.* **2024**, *162*, 171–185. [CrossRef]
22. Gisriel, C.J.; Brudvig, G.W. Investigations into Cyanobacterial Photoacclimation Processes Address Longstanding Proposals for Improving Crop Yields. *Nat. Commun.* **2025**, *16*, 3942. [CrossRef]

23. Elias, E.; Oliver, T.J.; Croce, R. Oxygenic Photosynthesis in Far-Red Light: Strategies and Mechanisms. *Annu. Rev. Phys. Chem.* **2024**, *75*, 231–256. [CrossRef]
24. Billi, D.; Napoli, A.; Mosca, C.; Fagliarone, C.; De Carolis, R.; Balbi, A.; Scanu, M.; Selinger, V.M.; Antonaru, L.A.; Nürnberg, D.J. Identification of Far-Red Light Acclimation in an Endolithic Chroococcidiopsis Strain and Associated Genomic Features: Implications for Oxygenic Photosynthesis on Exoplanets. *Front. Microbiol.* **2022**, *13*, 933404. [CrossRef] [PubMed]
25. Chen, M.; Blankenship, R.E. Expanding the Solar Spectrum Used by Photosynthesis. *Trends Plant Sci.* **2011**, *16*, 427–431. [CrossRef]
26. Kato, K.; Shinoda, T.; Nagao, R.; Akimoto, S.; Suzuki, T.; Dohmae, N.; Chen, M.; Allakhverdiev, S.I.; Shen, J.-R.; Akita, F.; et al. Structural Basis for the Adaptation and Function of Chlorophyll f in Photosystem I. *Nat. Commun.* **2020**, *11*, 238. [CrossRef]
27. Ho, M.-Y.; Gan, F.; Shen, G.; Zhao, C.; Bryant, D.A. Far-Red Light Photoacclimation (FaRLiP) in *Synechococcus* sp. PCC 7335: I. Regulation of FaRLiP Gene Expression. *Photosynth. Res.* **2017**, *131*, 173–186. [CrossRef] [PubMed]
28. Taniguchi, R.; Zhang, X.; Shinoda, T.; Tomo, T.; Ye, S.; Shibata, Y. The Reddest Fluorescence of Photosystem I from *Halomicronema hongdechloris* Comes from Chlorophyll-*f* Dimer. *J. Phys. Chem. B* **2025**, *129*, 6465–6476. [CrossRef] [PubMed]
29. Li, Y.; Scales, N.; Blankenship, R.E.; Willows, R.D.; Chen, M. Extinction Coefficient for Red-Shifted Chlorophylls: Chlorophyll d and Chlorophyll f. *Biochim. Biophys. Acta BBA—Bioenerg.* **2012**, *1817*, 1292–1298. [CrossRef]
30. Montgomery, B.L. Seeing New Light: Recent Insights into the Occurrence and Regulation of Chromatic Acclimation in Cyanobacteria. *Curr. Opin. Plant Biol.* **2017**, *37*, 18–23. [CrossRef]
31. Pinevich, A.V.; Averina, S.G. On the Edge of the Rainbow: Red-Shifted Chlorophylls and Far-Red Light Photoadaptation in Cyanobacteria. *Microbiology* **2022**, *91*, 631–648. [CrossRef]
32. Ho, M.-Y.; Soulier, N.T.; Canniffe, D.P.; Shen, G.; Bryant, D.A. Light Regulation of Pigment and Photosystem Biosynthesis in Cyanobacteria. *Curr. Opin. Plant Biol.* **2017**, *37*, 24–33. [CrossRef]
33. Mullineaux, C.W. How Do Cyanobacteria Sense and Respond to Light? *Mol. Microbiol.* **2001**, *41*, 965–971. [CrossRef]
34. Guergova-Kuras, M.; Boudreaux, B.; Joliot, A.; Joliot, P.; Redding, K. Evidence for Two Active Branches for Electron Transfer in Photosystem I. *Proc. Natl. Acad. Sci. USA* **2001**, *98*, 4437–4442. [CrossRef]
35. Shelaev, I.V.; Gostev, F.E.; Mamedov, M.D.; Sarkisov, O.M.; Nadtochenko, V.A.; Shuvalov, V.A.; Semenov, A.Y. Femtosecond Primary Charge Separation in *Synechocystis* sp. PCC 6803 Photosystem I. *Biochim. Biophys. Acta BBA—Bioenerg.* **2010**, *1797*, 1410–1420. [CrossRef] [PubMed]
36. Cherepanov, D.A.; Semenov, A.Y.; Mamedov, M.D.; Aybush, A.V.; Gostev, F.E.; Shelaev, I.V.; Shuvalov, V.A.; Nadtochenko, V.A. Current State of the Primary Charge Separation Mechanism in Photosystem I of Cyanobacteria. *Biophys. Rev.* **2022**, *14*, 805–820. [CrossRef] [PubMed]
37. Srinivasan, N.; Golbeck, J.H. Protein–Cofactor Interactions in Bioenergetic Complexes: The Role of the A1A and A1B Phylloquinones in Photosystem I. *Biochim. Biophys. Acta BBA—Bioenerg.* **2009**, *1787*, 1057–1088. [CrossRef] [PubMed]
38. Heathcote, P.; Jones, M.R.; Fyfe, P.K. Type I Photosynthetic Reaction Centres: Structure and Function. *Philos. Trans. R. Soc. Lond. B. Biol. Sci.* **2003**, *358*, 231–243. [CrossRef]
39. Hamaguchi, T.; Kawakami, K.; Shinzawa-Itoh, K.; Inoue-Kashino, N.; Itoh, S.; Ifuku, K.; Yamashita, E.; Maeda, K.; Yonekura, K.; Kashino, Y. Structure of the Far-Red Light Utilizing Photosystem I of *Acaryochloris marina*. *Nat. Commun.* **2021**, *12*, 2333. [CrossRef]
40. Ruprecht, J.; Iwata, S.; Rothery, R.A.; Weiner, J.H.; Maklashina, E.; Cecchini, G. Perturbation of the Quinone-Binding Site of Complex II Alters the Electronic Properties of the Proximal [3Fe-4S] Iron-Sulfur Cluster. *J. Biol. Chem.* **2011**, *286*, 12756–12765. [CrossRef]
41. Fu, H.-Y.; Picot, D.; Choquet, Y.; Longatte, G.; Sayegh, A.; Delacotte, J.; Guille-Collignon, M.; Lemaître, F.; Rappaport, F.; Wollman, F.-A. Redesigning the QA Binding Site of Photosystem II Allows Reduction of Exogenous Quinones. *Nat. Commun.* **2017**, *8*, 15274. [CrossRef]
42. Xu, C.; Zhu, Q.; Chen, J.; Shen, L.; Yi, X.; Huang, Z.; Wang, W.; Chen, M.; Kuang, T.; Shen, J.; et al. A Unique Photosystem I Reaction Center from a Chlorophyll *d*-containing Cyanobacterium *Acaryochloris marina*. *J. Integr. Plant Biol.* **2021**, *63*, 1740–1752. [CrossRef]
43. Miyashita, H.; Adachi, K.; Kurano, N.; Ikemot, H.; Chihara, M.; Miyach, S. Pigment Composition of a Novel Oxygenic Photosynthetic Prokaryote Containing Chlorophyll d as the Major Chlorophyll. *Plant Cell Physiol.* **1997**, *38*, 274–281. [CrossRef]
44. Averina, S.; Velichko, N.; Senatskaya, E.; Pinevich, A. Far-Red Light Photoadaptations in Aquatic Cyanobacteria. *Hydrobiologia* **2018**, *813*, 1–17. [CrossRef]
45. Ulrich, N.J.; Shen, G.; Bryant, D.A.; Miller, S.R. Ecological Diversification of a Cyanobacterium through Divergence of Its Novel Chlorophyll D-Based Light-Harvesting System. *Curr. Biol.* **2024**, *34*, 2972–2979.e4. [CrossRef] [PubMed]
46. Oliver, T.J.; Elias, E.; Croce, R. Acclimation to White Light in a Far-red Light Specialist: Insights from *Acaryochloris marina* MBIC11017. *New Phytol.* **2025**, *247*, 128–143. [CrossRef] [PubMed]

47. Mielke, S.P.; Kiang, N.Y.; Blankenship, R.E.; Gunner, M.R.; Mauzerall, D. Efficiency of Photosynthesis in a Chl D-Utilizing Cyanobacterium Is Comparable to or Higher than That in Chl a-Utilizing Oxygenic Species. *Biochim. Biophys. Acta BBA—Bioenerg.* **2011**, *1807*, 1231–1236. [CrossRef] [PubMed]
48. Reassessment of the Redox Potential of P740: The Primary Electron Donor in Photosystem I of the Chlorophyll d Containing Cyanobacterium, *Acaryochloris marina*. In *Photosynthesis. Energy from the Sun*; Springer: Dordrecht, The Netherlands, 2008; pp. 219–222. [CrossRef]
49. Tomo, T.; Allakhverdiev, S.I.; Mimuro, M. Constitution and Energetics of Photosystem I and Photosystem II in the Chlorophyll D-Dominated Cyanobacterium *Acaryochloris marina*. *J. Photochem. Photobiol. B* **2011**, *104*, 333–340. [CrossRef]
50. Linnanto, J.; Korppi-Tommola, J. Spectroscopic Properties of Mg-Chlorin, Mg-Porphin and Chlorophylls a, b, C1, C2, C3 and d Studied by Semi-Empirical and Ab Initio MO/CI Methods. *Phys. Chem. Chem. Phys.* **2000**, *2*, 4962–4970. [CrossRef]
51. Fiedor, L.; Kania, A.; Myśliwa-Kurdziel, B.; Orzeł, Ł.; Stochel, G. Understanding Chlorophylls: Central Magnesium Ion and Phytyl as Structural Determinants. *Biochim. Biophys. Acta BBA—Bioenerg.* **2008**, *1777*, 1491–1500. [CrossRef]
52. Bailleul, B.; Johnson, X.; Finazzi, G.; Barber, J.; Rappaport, F.; Telfer, A. The Thermodynamics and Kinetics of Electron Transfer between Cytochrome B6f and Photosystem I in the Chlorophyll D-Dominated Cyanobacterium, *Acaryochloris marina*. *J. Biol. Chem.* **2008**, *283*, 25218–25226. [CrossRef]
53. Tomo, T.; Kato, Y.; Suzuki, T.; Akimoto, S.; Okubo, T.; Noguchi, T.; Hasegawa, K.; Tsuchiya, T.; Tanaka, K.; Fukuya, M.; et al. Characterization of Highly Purified Photosystem I Complexes from the Chlorophyll D-Dominated Cyanobacterium *Acaryochloris marina* MBIC 11017. *J. Biol. Chem.* **2008**, *283*, 18198–18209. [CrossRef]
54. Nakamura, A.; Suzawa, T.; Kato, Y.; Watanabe, T. Species Dependence of the Redox Potential of the Primary Electron Donor P700 in Photosystem I of Oxygenic Photosynthetic Organisms Revealed by Spectroelectrochemistry. *Plant Cell Physiol.* **2011**, *52*, 815–823. [CrossRef]
55. Ohashi, S.; Kasahara, M.; Fukuyo, S.; Nakazato, M.; Iwamoto, K.; Shiraiwa, Y.; Kato, Y.; Watanabe, T. Redox Potential of Chlorophyll d. In *Photosynthesis. Energy from the Sun*; Springer: Dordrecht, The Netherlands, 2008; pp. 105–108. [CrossRef]
56. Kato, K.; Nagao, R.; Shen, J.R.; Miyazaki, N.; Akita, F. *Structure of PSI from H. hongdechloris Grown Under Far-Red Light Condition: 6kmx*; Protein Data Bank: Cambridge, UK, 2020. [CrossRef]
57. Gisriel, C.J.; Wang, J. *Quantitative Assessment of Chlorophyll Types in Cryo-EM Maps of Photosystem I Acclimated to Far-Red Light: 7lx0*; Protein Data Bank: Cambridge, UK, 2021. [CrossRef]
58. Wlodawer, A.; Minor, W.; Dauter, Z.; Jaskolski, M. Protein Crystallography for Non-crystallographers, or How to Get the Best (but Not More) from Published Macromolecular Structures. *FEBS J.* **2008**, *275*, 1–21. [CrossRef] [PubMed]
59. Webber, A.N.; Su, H.; Bingham, S.E.; Käss, H.; Krabben, L.; Kuhn, M.; Jordan, R.; Schlodder, E.; Lubitz, W. Site-Directed Mutations Affecting the Spectroscopic Characteristics and Midpoint Potential of the Primary Donor in Photosystem I. *Biochemistry* **1996**, *35*, 12857–12863. [CrossRef] [PubMed]
60. Ivancich, A.; Mattioli, T.A.; Artz, K.; Wang, S.; Allen, J.P.; Williams, J.C. Influence of Asn/His L166 on the Hydrogen-Bonding Pattern and Redox Potential of the Primary Donor of Purple Bacterial Reaction Centers. *Biochemistry* **1997**, *36*, 3027–3036. [CrossRef]
61. Ivancich, A.; Artz, K.; Williams, J.C.; Allen, J.P.; Mattioli, T.A. Effects of Hydrogen Bonds on the Redox Potential and Electronic Structure of the Bacterial Primary Electron Donor. *Biochemistry* **1998**, *37*, 11812–11820. [CrossRef]
62. Saito, K.; Ishikita, H. Cationic State Distribution over the P700 Chlorophyll Pair in Photosystem I. *Biophys. J.* **2011**, *101*, 2018–2025. [CrossRef]
63. Hastings, G.; Wang, R. Vibrational Mode Frequency Calculations of Chlorophyll-d for Assessing (P740+-P740) FTIR Difference Spectra Obtained Using Photosystem I Particles from *Acaryochloris marina*. *Photosynth. Res.* **2007**, *95*, 55–62. [CrossRef]
64. Mino, H.; Kawamori, A.; Aoyama, D.; Tomo, T.; Iwaki, M.; Itoh, S. Proton ENDOR Study of the Primary Donor P740+, a Special Pair of Chlorophyll d in Photosystem I Reaction Center of *Acaryochloris marina*. *Chem. Phys. Lett.* **2005**, *411*, 262–266. [CrossRef]
65. Petrova, A.A.; Casazza, A.P.; Shelaev, I.V.; Gostev, F.E.; Aybush, A.V.; Nadtochenko, V.A.; Semenov, A.Y.; Santabarbara, S.; Cherepanov, D.A. Role of Pheophytin a in the Primary Charge Separation of Photosystem I from *Acaryochloris marina*: Femtosecond Optical Studies of Excitation Energy and Electron Transfer Reactions. *Biochim. Biophys. Acta BBA—Bioenerg.* **2023**, *1864*, 148984. [CrossRef]
66. Cohen, R.O.; Shen, G.; Golbeck, J.H.; Xu, W.; Chitnis, P.R.; Valieva, A.I.; Van Der Est, A.; Pushkar, Y.; Stehlik, D. Evidence for Asymmetric Electron Transfer in Cyanobacterial Photosystem I: Analysis of a Methionine-to-Leucine Mutation of the Ligand to the Primary Electron Acceptor A_0. *Biochemistry* **2004**, *43*, 4741–4754. [CrossRef] [PubMed]
67. Dashdorj, N.; Xu, W.; Cohen, R.O.; Golbeck, J.H.; Savikhin, S. Asymmetric Electron Transfer in Cyanobacterial Photosystem I: Charge Separation and Secondary Electron Transfer Dynamics of Mutations Near the Primary Electron Acceptor A0. *Biophys. J.* **2005**, *88*, 1238–1249. [CrossRef] [PubMed]

68. McConnell, M.D.; Sun, J.; Siavashi, R.; Webber, A.; Redding, K.E.; Golbeck, J.H.; Van Der Est, A. Species-Dependent Alteration of Electron Transfer in the Early Stages of Charge Stabilization in Photosystem I. *Biochim. Biophys. Acta BBA—Bioenerg.* **2015**, *1847*, 429–440. [CrossRef] [PubMed]
69. Noji, T.; Saito, K.; Ishikita, H. How the Electron-Transfer Cascade Is Maintained in Chlorophyll-*d* Containing Photosystem I. *Biochemistry* **2025**, *64*, 203–212. [CrossRef]
70. Kato, K.; Hamaguchi, T.; Nagao, R.; Kawakami, K.; Ueno, Y.; Suzuki, T.; Uchida, H.; Murakami, A.; Nakajima, Y.; Yokono, M.; et al. Structural Basis for the Absence of Low-Energy Chlorophylls in a Photosystem I Trimer from Gloeobacter Violaceus. *eLife* **2022**, *11*, e73990. [CrossRef]
71. Chen, M.; Schliep, M.; Willows, R.D.; Cai, Z.-L.; Neilan, B.A.; Scheer, H. A Red-Shifted Chlorophyll. *Science* **2010**, *329*, 1318–1319. [CrossRef]
72. Chen, M.; Li, Y.; Birch, D.; Willows, R.D. A Cyanobacterium That Contains Chlorophyll *f*—A Red-absorbing Photopigment. *FEBS Lett.* **2012**, *586*, 3249–3254. [CrossRef]
73. Chen, M.; Hernandez-Prieto, M.A.; Loughlin, P.C.; Li, Y.; Willows, R.D. Genome and Proteome of the Chlorophyll F-Producing Cyanobacterium Halomicronema Hongdechloris: Adaptative Proteomic Shifts under Different Light Conditions. *BMC Genom.* **2019**, *20*, 207. [CrossRef]
74. Gan, F.; Zhang, S.; Rockwell, N.C.; Martin, S.S.; Lagarias, J.C.; Bryant, D.A. Extensive Remodeling of a Cyanobacterial Photosynthetic Apparatus in Far-Red Light. *Science* **2014**, *345*, 1312–1317. [CrossRef]
75. Nürnberg, D.J.; Morton, J.; Santabarbara, S.; Telfer, A.; Joliot, P.; Antonaru, L.A.; Ruban, A.V.; Cardona, T.; Krausz, E.; Boussac, A.; et al. Photochemistry beyond the Red Limit in Chlorophyll f–Containing Photosystems. *Science* **2018**, *360*, 1210–1213. [CrossRef]
76. Shen, G.; Canniffe, D.P.; Ho, M.-Y.; Kurashov, V.; Van Der Est, A.; Golbeck, J.H.; Bryant, D.A. Characterization of Chlorophyll f Synthase Heterologously Produced in *Synechococcus* sp. PCC 7002. *Photosynth. Res.* **2019**, *140*, 77–92. [CrossRef] [PubMed]
77. Zhao, C.; Gan, F.; Shen, G.; Bryant, D.A. RfpA, RfpB, and RfpC Are the Master Control Elements of Far-Red Light Photoacclimation (FaRLiP). *Front. Microbiol.* **2015**, *6*, 1303. [CrossRef]
78. Gisriel, C.J.; Cardona, T.; Bryant, D.A.; Brudvig, G.W. Molecular Evolution of Far-Red Light-Acclimated Photosystem II. *Microorganisms* **2022**, *10*, 1270. [CrossRef]
79. Hastings, G.; Makita, H.; Agarwala, N.; Rohani, L.; Shen, G.; Bryant, D.A. Fourier Transform Visible and Infrared Difference Spectroscopy for the Study of P700 in Photosystem I from Fischerella Thermalis PCC 7521 Cells Grown under White Light and Far-Red Light: Evidence That the A–1 Cofactor Is Chlorophyll f. *Biochim. Biophys. Acta BBA—Bioenerg.* **2019**, *1860*, 452–460. [CrossRef]
80. Cherepanov, D.A.; Shelaev, I.V.; Gostev, F.E.; Aybush, A.V.; Mamedov, M.D.; Shen, G.; Nadtochenko, V.A.; Bryant, D.A.; Semenov, A.Y.; Golbeck, J.H. Evidence That Chlorophyll f Functions Solely as an Antenna Pigment in Far-Red-Light Photosystem I from Fischerella Thermalis PCC 7521. *Biochim. Biophys. Acta BBA—Bioenerg.* **2020**, *1861*, 148184. [CrossRef]
81. Gisriel, C.; Shen, G.; Kurashov, V.; Ho, M.-Y.; Zhang, S.; Williams, D.; Golbeck, J.H.; Fromme, P.; Bryant, D.A. The Structure of Photosystem I Acclimated to Far-Red Light Illuminates an Ecologically Important Acclimation Process in Photosynthesis. *Sci. Adv.* **2020**, *6*, eaay6415. [CrossRef]
82. Kaucikas, M.; Nürnberg, D.; Dorlhiac, G.; Rutherford, A.W.; Van Thor, J.J. Femtosecond Visible Transient Absorption Spectroscopy of Chlorophyll f-Containing Photosystem I. *Biophys. J.* **2017**, *112*, 234–249. [CrossRef]
83. Zamzam, N.; Kaucikas, M.; Nürnberg, D.J.; Rutherford, A.W.; Van Thor, J.J. Femtosecond Infrared Spectroscopy of Chlorophyll F-Containing Photosystem I. *Phys. Chem. Chem. Phys.* **2019**, *21*, 1224–1234. [CrossRef] [PubMed]
84. Gisriel, C.J.; Huang, H.-L.; Reiss, K.M.; Flesher, D.A.; Batista, V.S.; Bryant, D.A.; Brudvig, G.W.; Wang, J. Quantitative Assessment of Chlorophyll Types in Cryo-EM Maps of Photosystem I Acclimated to Far-Red Light. *BBA Adv.* **2021**, *1*, 100019. [CrossRef] [PubMed]
85. Li, Y.; Vella, N.; Chen, M. Characterization of Isolated Photosystem I from Halomicronema Hongdechloris, a Chlorophyll f-Producing Cyanobacterium. *Photosynthetica* **2018**, *56*, 306–315. [CrossRef]
86. Vasil'ev, S.; Shen, J.-R.; Kamiya, N.; Bruce, D. The Orientations of Core Antenna Chlorophylls in Photosystem II Are Optimized to Maximize the Quantum Yield of Photosynthesis. *FEBS Lett.* **2004**, *561*, 111–116. [CrossRef] [PubMed]
87. Käss, H.; Fromme, P.; Witt, H.T.; Lubitz, W. Orientation and Electronic Structure of the Primary Donor Radical Cation in Photosystem I: A Single Crystals EPR and ENDOR Study. *J. Phys. Chem. B* **2001**, *105*, 1225–1239. [CrossRef]
88. Schmitt, F.-J.; Friedrich, T. Adaptation Processes in Halomicronema Hongdechloris, an Example of the Light-Induced Optimization of the Photosynthetic Apparatus on Hierarchical Time Scales. *Front. Plant Sci.* **2024**, *15*, 1359195. [CrossRef] [PubMed]
89. Schmitt, F.-J.; Campbell, Z.Y.; Bui, M.V.; Hüls, A.; Tomo, T.; Chen, M.; Maksimov, E.G.; Allakhverdiev, S.I.; Friedrich, T. Photosynthesis Supported by a Chlorophyll F-Dependent, Entropy-Driven Uphill Energy Transfer in Halomicronema Hongdechloris Cells Adapted to Far-Red Light. *Photosynth. Res.* **2019**, *139*, 185–201. [CrossRef] [PubMed]

90. Gisriel, C.J.; Shen, G.; Kurashov, V.; Ho, M.; Zhang, S.; Williams, D.; Golbeck, J.H.; Fromme, P.; Bryant, D.A. *Structure of Photosystem I Acclimated to Far-Red Light: 6pnj*; Protein Data Bank: Cambridge, UK, 2020; 6p. [CrossRef]
91. Jordan, P.; Fromme, P.; Witt, H.T.; Klukas, O.; Saenger, W.; Krauss, N. *Crystal Structure of Photosystem I: A Photosynthetic Reaction Center and Core Antenna System from Cyanobacteria: 1jb0*; Protein Data Bank: Cambridge, UK, 2001. [CrossRef]

Disclaimer/Publisher's Note: The statements, opinions and data contained in all publications are solely those of the individual author(s) and contributor(s) and not of MDPI and/or the editor(s). MDPI and/or the editor(s) disclaim responsibility for any injury to people or property resulting from any ideas, methods, instructions or products referred to in the content.